Interpreting the Ultraviolet Aerosol Index Observed with the OMI Satellite Instrument to Understand Absorption by Organic Aerosols: Implications for Atmospheric Oxidation and Direct Radiative Effects

Melanie S. Hammer[1], Randall V. Martin[1,2], Aaron van Donkelaar[1], Virginie Buchard[3,4], Omar Torres[3], David A. Ridley[5], Robert J.D. Spurr[6]

[1]Department of Physics and Atmospheric Science, Dalhousie University, Canada

[2]Harvard-Smithsonian Center for Astrophysics, Cambridge, MA, USA

[3]NASA/Goddard Space Flight Center, Greenbelt, MD, USA

[4]GESTAR/Universities Space Research Association, Columbia, MD, USA

[5]Department of Civil and Environmental Engineering, Massachusetts Institute of Technology, Cambridge, MA, USA

[6]RT Solutions, Inc., 9 Channing Street, Cambridge, MA 02138, USA

Correspondence to: M. S. Hammer (melanie.hammer@dal.ca)

Abstract

Satellite observations of the Ultraviolet Aerosol Index (UVAI) are sensitive to absorption of solar radiation by aerosols; this absorption affects photolysis frequencies and radiative forcing. We develop a global simulation of the UVAI using the 3-D chemical transport model GEOS-Chem coupled with the Vector Linearized Discrete Ordinate Radiative Transfer model (VLIDORT). The simulation is applied to interpret UVAI observations from the Ozone Monitoring Instrument (OMI) for the year 2007. Simulated and observed values are highly consistent in regions where mineral dust dominates the UVAI, but a large negative bias (-0.32 to -0.97) exists between simulated and observed values in biomass burning regions. We determine effective optical properties for absorbing organic aerosol, known as brown carbon (BrC), and implement them into GEOS-Chem to better represent observed UVAI values over biomass burning regions. The inclusion of absorbing BrC decreases the mean bias between simulated and OMI UVAI values from -0.57 to -0.09 over West Africa in January, from -0.32 to +0.0002 over South Asia in April, from -0.97 to -0.22 over southern Africa in July, and from -0.50 to +0.33 over South America in

September. The spectral dependence of absorption after including BrC in the model is broadly consistent with reported observations for biomass burning aerosol, with Absorbing Angstrom Exponent (AAE) values ranging from 2.9 in the ultraviolet (UV) to 1.3 across the UV-Near IR spectrum. We assess the effect of the additional UV absorption by BrC on atmospheric photochemistry by examining tropospheric hydroxyl radical (OH) concentrations in GEOS-Chem. The inclusion of BrC decreases OH by up to 30% over South America in September, up to 20% over southern Africa in July, and up to 15% over other biomass burning regions. Global annual mean OH concentrations in GEOS-Chem decrease due to the presence of absorbing BrC, increasing the methyl chloroform lifetime from 5.62 years to 5.68 years, thus reducing the bias against observed values. We calculate the direct radiative effect (DRE) of BrC using GEOS-Chem coupled with the radiative transfer model RRTMG (GC-RT). Treating organic aerosol as containing more strongly absorbing BrC changes the global annual mean all-sky top of atmosphere (TOA) DRE by +0.03 W m^{-2} and all-sky surface DRE by -0.08 W m^{-2}. Regional changes of up to +0.3 W m^{-2} at TOA and down to -1.5 W m^{-2} at the surface are found over major biomass burning regions.

1 Introduction

Absorption of solar radiation by aerosols plays a major role in radiative forcing and atmospheric photochemistry. Aerosol absorption has been estimated to be the second largest source of radiative forcing after carbon dioxide (Bond et al., 2013; IPCC, 2014; Ramanathan and Carmichael, 2008), although considerable uncertainty remains regarding the magnitude of the forcing (Stier et al., 2007; Wang et al., 2014). Absorption of ultraviolet (UV) radiation by aerosols decreases photolysis frequencies, leading to a reduction in the concentrations of atmospheric oxidants (Dickerson et al., 1997; Jacobson, 1998; Liao et al., 2003; Martin et al., 2003). Many atmospheric chemistry models tend to overestimate tropospheric hydroxyl radical (OH) concentrations compared to observations (Mao et al., 2013; Naik et al., 2013). Accurately representing aerosol absorption could help rectify the discrepancies between simulated and observed OH concentrations, and offer constraints on radiative forcing.

The Ultraviolet Aerosol Index (UVAI) is a method of detecting aerosol absorption using satellite measurements. The UVAI is calculated by separating the spectral contrast of radiances due to aerosol effects from those due to Rayleigh scattering at two wavelengths in the near-UV

region (Herman et al., 1997; Torres et al., 1998, 2007). Two attributes of the UVAI method are 1) that aerosol optical properties are more readily detected over surfaces with low reflectance such as found in the UV (Torres et al., 2005), and 2) that the strong interaction between aerosol absorption and molecular scattering in the near-UV increases the sensitivity of UV-radiances to aerosol absorption (Torres et al., 1998). These attributes enhance the ability of the UVAI to detect aerosol absorption that affects UV photolysis and radiative forcing.

Traditionally, black carbon (BC) is treated as the predominant absorbing carbonaceous aerosol, and all organic carbon is assumed to be primarily scattering or weakly absorbing colorless aerosol. However, a growing number of observations have found evidence of significant absorption by a subset of organic carbon, known as "brown carbon" (BrC), which is strongest in the ultraviolet and decreases into the visible and near-IR wavelength regions (Bergstrom et al., 2007; Chen and Bond, 2010; Kirchstetter et al., 2004; Martins et al., 2009; Yang et al., 2008; Zhong and Jang, 2014). The majority of BrC is emitted to the atmosphere through low-temperature, incomplete combustion of biomass and biofuel (Chen and Bond, 2010; Kirchstetter et al., 2004; Zhong and Jang, 2014). There is evidence of a possible source from residential coal burning (Bond, 2001), while the high-temperature environment associated with other fossil fuel combustion is unfavorable to BrC formation (Andreae and Gelencsér, 2006; Saleh et al., 2014). BrC has been observed to contribute significantly to the overall absorption by biomass burning aerosol, especially in the UV (Clarke et al., 2007; Corr et al., 2012; Kirchstetter and Thatcher, 2012). The UVAI is sensitive to this absorption (Jethva and Torres, 2011).

A great deal of uncertainty exists regarding the fraction of total primary organic carbon that is brown (BrC/POC). This uncertainty arises from the variety of methods used to measure BrC absorption as well as the variable nature of organic aerosols themselves (Lack and Langridge, 2013). Filter-based measurements where the organic carbon is extracted from the total biomass burning aerosol sample with the use of solvents range from 50-90% (Chen and Bond, 2010; Kirchstetter et al., 2004). A broad range of BrC/POC values have been used to simulate absorption by brown carbon. For example, Feng et al. (2013) assume 66% of primary organic carbon from biomass and biofuel emissions is brown, Wang et al. (2014) assume 50% of POC from biomass and 25% of POC from biofuel emissions is brown, while Lin et al. (2014) assume 100% POC from

biomass and biofuel emissions is brown. Global observations of reflected solar radiation used in the UVAI could offer a constraint on these different assumptions.

Several estimates of BrC absorption exist, but they all differ significantly. The imaginary part of the refractive index (k) for BrC derived by Kirchstetter et al. (2004) and Chen and Bond (2010) are often taken, respectively, as the upper ($k \sim 0.168$ at 350 nm) and lower ($k \sim 0.074$ at 350 nm) limits in modelling studies (Arola et al., 2011; Feng et al., 2013; Lin et al., 2014). Different observations may reflect different burn conditions (Saleh et al., 2014) as well as chemical loss and evaporation of BrC (Forrister et al., 2015; Zhong and Jang, 2014). Global observations are needed to infer the effective absorption across a variety of conditions. Many studies have estimated the direct radiative effect (DRE) and/or direct radiative forcing (DRF) by BrC. In Heald et al. (2014) a clear distinction is made between the DRE, which is the instantaneous imbalance of out-going longwave and incoming shortwave radiation due to the presence of an atmospheric constituent, and the DRF, which is the difference in DRE between present-day and preindustrial conditions. Prior estimates of the change in all-sky top of atmosphere (TOA) DRE from treating organic aerosol as containing BrC range from +0.04 W m^{-2} to +0.25 W m^{-2} globally (Chung et al., 2012; Feng et al., 2013), with estimates of regional seasonal DRE of organic aerosol including absorbing BrC ranging from +0.5-1 W m^{-2} (Arola et al., 2015). Most studies estimate a TOA DRF between 0.07 and 0.57 W m^{-2} due to absorption by BrC (Lin et al., 2014; Park et al., 2010; Wang et al., 2014). Following submission of our manuscript, we learned of a submitted manuscript by Jo et al., (2015) that developed a global simulation of BrC and applied it to investigate atmospheric photochemistry. To our knowledge, this work and that by Jo et al., (2015) are the first two chemical transport modeling studies that have considered the effect of absorption by BrC on atmospheric photochemistry.

In this work we introduce brown carbon to the chemical transport model GEOS-Chem and examine its effect on atmospheric absorption and photochemistry, in particular in known biomass burning regions. To evaluate aerosol absorption, section 3 develops a simulation of the UVAI following Buchard et al. (2015) using the Vector Linearized Discrete Radiative Transfer model (VLIDORT) coupled with aerosol fields from GEOS-Chem. Section 4 compares the simulated UVAI values to observations from the Ozone Monitoring Instrument (OMI). The change in reflected solar radiation as observed by the UVAI tests the effective representation of the

absorption of UV radiation by BrC. Section 5 examines the effect of the added BrC absorption on ozone photolysis frequencies and tropospheric OH concentrations in the GEOS-Chem simulation. Section 6 calculates the DRE of absorbing brown carbon. Section 7 reports the conclusions.

2 Observations

2.1 OMI Ultraviolet Aerosol Index

The OMI Ultraviolet Aerosol Index is a method of detecting absorbing aerosols from satellite measurements in the near-UV wavelength region. The UVAI was first observed from the Nimbus-7 TOMS (Total Ozone Mapping Spectrometer) (Herman et al., 1997; Torres et al., 1998) and is currently a product of the OMI Near-UV algorithm (OMAERUV) (Torres et al., 2007). OMI flies on NASA's Aura satellite and has been taking global daily measurements since 2004. The OMAERUV algorithm uses the 354 and 388 nm radiances measured by OMI to calculate the UVAI according to Torres et al. (1998, 2007):

$$\mathrm{UVAI} = -100 \log_{10}\left[\frac{I_{354}^{\mathrm{meas}}}{I_{354}^{\mathrm{calc}}\left(R_{354}^{*}\right)}\right] \quad (1)$$

where I_{354}^{meas} is the TOA at 354 nm as measured by OMI, and I_{354}^{calc} is the radiance at 354 nm calculated for a purely Rayleigh scattering atmosphere bounded by a Lambertian surface of reflectance R_{354}^{*}, which is known as the adjusted Lambert Equivalent Reflectivity (LER) (Dave, 1978). R_{354}^{*} is calculated by correcting the LER at 388 nm (R_{388}^{*}) for the spectral dependence of the surface reflectance at 354 nm.

Positive UVAI values indicate absorbing aerosol. Negative values indicate non-absorbing aerosol. Near-zero values indicate clouds, minimal aerosol, or other non-aerosol related effects such as unaccounted for land surface albedo wavelength dependence, ocean color effects or specular ocean reflection (i.e. sun glint). These second order effects yield UVAI values ± 0.5 within the noise level (Torres et al., 2007). The OMAERUV product identifies clouds using the measured scene reflectivity and the UVAI (Torres et al., 2013). We reject cloudy conditions (quality flag of 1) to focus on cloud free conditions (quality flag 0).

In this work we use the OMI UVAI to evaluate simulated UVAI values, as described in section 3.

2.2 Absorption Angstrom Exponent (AAE)

We use observations of the Absorption Angstrom Exponent (AAE) for biomass burning aerosol to test our representation of the spectral dependence of absorption. The AAE is the slope of aerosol absorption optical depth (AAOD) versus wavelength (λ) in log-log space. Using the AAE, the AAOD can be related to wavelength with the power-law relationship

$$\mathrm{AAOD} = k\lambda^{-\mathrm{AAE}} \quad (2),$$

where k is a constant. Aerosols with spectrally independent absorption display an AAE of about 1, while aerosols with spectrally dependent absorption have an AAE > 1. BC exhibits spectrally independent absorption, and is often accepted as having an AAE close to 1 (Bergstrom et al., 2002; Bond and Bergstrom, 2006). The observed AAE over the near-UV to near-IR spectral regions can indicate aerosol type, with urban pollution aerosols dominated by BC exhibiting an AAE near 1, biomass burning aerosols displaying an AAE near 2, and desert dust having an AAE > 2 (Bergstrom et al., 2007; Russell et al., 2009).

Several recent studies have attributed the spectrally dependent absorption by biomass burning aerosols to the presence of BrC (Clarke et al., 2007; Corr et al., 2012; Kirchstetter and Thatcher, 2012; Rizzo et al., 2011; Zhong and Jang, 2014). Kirchstetter et al. (2004) measured over the 300-1000 nm range an AAE of ~ 2 for biomass burning aerosol and an AAE of ~ 1 for motor vehicle aerosol. They found that after extracting the organic carbon from the samples using acetone, the AAE of the biomass burning aerosol decreased to around 1, while the motor vehicle aerosol AAE remained unchanged. They concluded that the spectral dependence of absorption by biomass burning aerosol was due to BrC, while the absorption by motor vehicle emissions was due to BC.

Table 1 contains a summary of measured AAE values for biomass burning aerosol. AAE values increase toward UV wavelengths as expected for BrC absorption. Variability in the AAE at visible wavelengths may reflect differences in burn conditions and fuel type. Observations in the ultraviolet, such as the UVAI, offer an exciting opportunity to exploit the large AAE of biomass burning aerosol at short wavelengths to assess the global magnitude of BrC absorption (Jethva and Torres, 2011).

3. Simulated Ultraviolet Aerosol Index

We simulate the UVAI following Buchard et al. (2015) using the VLIDORT model (Spurr, 2006), which includes polarization effects and uses the discrete ordinates method to solve the radiative transfer equation. We supply VLIDORT with the OMI pixel viewing geometry to calculate the UVAI for that pixel. The UVAI values are calculated from TOA radiances computed by VLIDORT at 354 and 388 nm, the wavelengths used by the OMAERUV product.

Following Buchard et al. (2015) we calculate simulated UVAI values as:

$$\mathrm{UVAI} = -100 \log_{10}\left[\frac{I_{354}^{\mathrm{RAY+AER}}}{I_{354}^{\mathrm{RAY}}\left(R_{354}^{*}\right)}\right] \tag{3}$$

where $I_{354}^{\mathrm{RAY+AER}}$ is the TOA radiance calculated with VLIDORT at 354 nm assuming an atmosphere containing aerosol and Rayleigh effects, and I_{354}^{RAY} is the TOA radiance calculated with VLIDORT at 354 nm assuming a purely Rayleigh scattering atmosphere bounded by a Lambertian surface of reflectance R_{354}^{*} (adjusted Lambert Equivalent Reflectivity).

R_{354}^{*} is calculated by correcting the Lambert Equivalent Reflectivity at 388 nm (R_{388}^{*}) for wavelength dependence:

$$R_{354}^{*} = R_{388}^{*} - (R_{388} - R_{354}) \tag{4}$$

where R_{388} and R_{354} are surface reflectance values from a revisited TOMS-based climatology dataset (Torres et al., 2013).

R_{388}^{*} is calculated by relating TOA radiance to diffuse reflectivity using the equation (Buchard et al., 2015):

$$R_{388}^{*} = \frac{I_{388}^{\mathrm{RAY+AER}} - I_{388}^{\mathrm{RAY}}}{T_{388}^{\mathrm{RAY}} + S_{b388}^{\mathrm{RAY}}\left(I_{388}^{\mathrm{RAY+AER}} - I_{388}^{\mathrm{RAY}}\right)} \tag{5}$$

where $I_{388}^{\mathrm{RAY+AER}}$ is the TOA radiance calculated with VLIDORT at 388 nm assuming an atmosphere containing aerosol and Rayleigh effects, I_{388}^{RAY} is the TOA radiance at 388 nm calculated with VLIDORT for a purely Rayleigh scattering atmosphere bounded by a Lambertian

surface, T_{388}^{RAY} is the simulated transmittance at 388 nm for a Rayleigh atmosphere, and S_{b388}^{RAY} is the spherical albedo of a Rayleigh atmosphere at 388 nm.

For the calculation of TOA radiances, we provide VLIDORT with vertical profiles of aerosol extinction, single scattering albedo, and 32 Legendre-function expansion coefficients of the scattering phase function. We assume all aerosol particles are spherical. We obtain these aerosol optical properties using daily aerosol fields at satellite overpass time from GEOS-Chem version 9-01-03 (http://geos-chem.org), a global three dimensional chemical transport model driven by assimilated meteorological data from the Goddard Earth Observation System (GEOS-5) of the NASA Global Modeling and Assimilation Office (GMAO). Our simulation is conducted at a spatial resolution of 2°x2.5° with 47 vertical levels for the year 2007.

GEOS-Chem contains a detailed oxidant-aerosol chemical mechanism (Bey et al., 2001; Park et al., 2004). The aerosol simulation includes the sulfate-nitrate-ammonium system (Fountoukis and Nenes, 2007; Park et al., 2004; Pye et al., 2009), primary carbonaceous aerosol (Park et al., 2003), mineral dust (Fairlie et al., 2007), and sea salt (Jaeglé et al., 2011). Aerosol optical properties are based on the Global Aerosol Data Set (GADS) (Köepke et al., 1997) as implemented by Martin et al., (2003), with updates for organics and secondary inorganics from aircraft observations (Drury et al., 2010), and for mineral dust (Lee et al., 2009; Ridley et al., 2012). Aerosols are treated as externally mixed. We treat the density of organic aerosol as 1.3 g cm^{-3} (Duplissy et al., 2011; Kuwata et al., 2012) and assume an organic aerosol mass to organic carbon fraction of 2.1 (Aiken et al., 2008; Canagaratna et al., 2015; Turpin and Lim, 2001).

Anthropogenic emissions are from the EDGAR v32-FT2000 global inventory for 2000 (Olivier et al., 2005) with emissions overwritten in areas with regional inventories for the United States (NEI 2005), Mexico (BRAVO; Kuhns et al., 2005), Europe (EMEP; http://www.emep.int/), and East Asia (Zhang et al., 2009). Emissions are scaled to the year 2007 following emissions of related CO_2 sources as described in van Donkelaar et al. (2008). Global biofuel emissions (Yevich and Logan, 2003), global anthropogenic emissions for carbonaceous aerosols (Bond et al., 2007; Leibensperger et al., 2012), and emissions from open fires for individual years from the GFED3 inventory (Mu et al., 2011) are included.

We calculate UVAI values for two cases. The base case simulation treats the aerosol optical properties as currently implemented in GEOS-Chem in which all organic carbon aerosols are weakly absorbing and colorless as shown in Table 2. The second case adds the more strongly absorbing BrC as described in section 4.2 below.

4 Comparison of simulated and OMI UVAI

4.1 Base case simulation

Figure 1 shows the monthly mean OMI UVAI observations for January, April, July, and September of 2007. Clear signals are apparent over regions dominated by mineral dust and biomass burning (Herman et al., 1997; Torres et al., 1998). Absorption over desert regions occurs for all four months, giving UVAI values between 1 and 3, particularly over the Saharan, Iranian, and Thar deserts. Aerosol absorption from biomass burning primarily follows the seasonal cycle of agricultural burning (Duncan et al., 2003). In January, absorption over West Africa yields UVAI values between 1 and 2.5. In April aerosol absorption is visible over South Asia with UVAI values between 0.5 and 1. UVAI values of 1-1.7 occur over southern Africa in both July and September, while UVAI values of up to 3 occur over South America in September.

Figure 2 shows the monthly mean UVAI values for our base case simulation without BrC.. The simulation captures the major absorption features compared to OMI over the desert regions, giving UVAI values of 1-3, however it fails to capture the absorption by biomass burning aerosol, giving UVAI values between -2 and 0 in all biomass burning regions for the four months. These negative values indicate that the UVAI simulation is insensitive to the absorption by BC and is dominated by the scattering from organic carbon aerosol. A sensitivity test with doubled BC concentrations increased UVAI values by only ~0.1. We also conducted a sensitivity test to determine if the heights of the biomass burning plumes could explain the underestimated absorption. Raising the aerosol layer height to unrealistic altitudes (~10 km above the surface) increased the UVAI by only 0.1-0.3, which is insufficient to account for the differences between the simulation and observations.

To further analyze the discrepancies between simulated and observed UVAI, we choose four regions corresponding to the seasonal biomass burning outlined in Figure 1: West Africa (5°S-25°N, 40°W-20°E) in January, South Asia (5-35°N, 60-110°E) in April, southern Africa (0-30°S,

5°W-30°E) in July, and South America (0-40°S, 40-70°W) in September. Table 3 contains the correlation coefficients (r) between the simulated and OMI UVAI as well as the mean bias (simulated-OMI UVAI). The correlation between the OMI and simulated UVAI is low (0.09-0.48) in all regions, with large mean biases of -0.32 to -0.97

Uncertainty in aerosol optical depth also cannot explain the UVAI bias. Table 4 shows the simulated AOD compared with AOD retrieved from the MODIS (Moderate Resolution Imaging Spectroradiometer) and MISR (Multi-angle Imaging Spectroradiometer) satellite instruments. Overall the simulated values are within the range of satellite retrieved AOD values. The maximum difference in simulated versus satellite AOD is found with the MODIS Dark Target algorithm over South America in September. Matching the simulated AOD to the satellite AOD changed the UVAI by less than 0.1.

We attempt to reconcile the differences between the simulated and OMI UVAI in biomass burning regions by introducing absorbing BrC into GEOS-Chem, as described below.

4.2 Treatment of brown carbon

Here we apply the OMI UVAI observations to estimate the effective absorption by BrC. We exploit the fact that the TOA radiances used in the OMI UVAI contain implicit information on the BrC from actual burn conditions, on the BrC that remains after chemical loss or evaporation, on Br-SOA, and on the BrC/POC fraction. We use the term effective to denote the implicit dependence of the UVAI upon these multiple processes. Through sensitivity simulations, we derive the effective k values for BrC given the assumed BrC/POC fraction required to reproduce the observed absorption by the OMI UVAI. This is accomplished by conducting the sensitivity simulations for several cases of BrC/POC fraction, assuming the same fixed spectral dependence for each case, and adjusting the magnitude of the effective k values to match the OMI UVAI. We treat the relative spectral dependence of k, $\log(\Delta k)/\log(\Delta\lambda)$, as 3 for wavelengths between 300 and 600 nm to represent the mean from laboratory and field measurements of 3.2 ± 0.7 (Kirchstetter et al., 2004; Zhang et al., 2013; Zhong and Jang, 2014). At wavelengths ≥ 600 nm we leave the absorption properties of POC unchanged since BrC absorption decreases significantly into the visible and near-IR (Bergstrom et al., 2007; Chen and Bond, 2010; Yang et al., 2008).

The filled circles in Figure 3 show the effective k values of BrC derived from seven sensitivity simulations that all achieve the same simulated UVAI. Only the BrC/POC fraction varies between simulations. The choice of simulated UVAI was selected to represent the global OMI UVAI over major biomass burning regions. The imaginary part of the refractive index decreases with increasing wavelength following an exponential relationship as prescribed based on laboratory and field measurements, and decreases with increasing BrC/POC fraction as required to reproduce the OMI UVAI. The effective k values increase with decreasing BrC/POC fraction because as BrC concentration decreases, BrC must be more absorbing to match the absorption observed by OMI. Given the smoothly varying relationship between k and BrC/POC we develop the following expression to represent this relationship:

$$k = c \cdot \rho \cdot \lambda \cdot \left[35.4 \left(\frac{BrC}{POC}\right)^{-1.25} \cdot \exp(-10.5\lambda)\right] ; \text{BrC/POC} \geq 0.4, 300 \text{ nm} \leq \lambda \leq 600 \text{ nm} \quad (6),$$

where λ is wavelength (μm), ρ is the density of organic carbon (g μm^{-3}), and c is a conversion constant equal to $1.0 \times 10^{12}/4\pi$ μm^2 g^{-1}.

The background spectrum of Figure 3 shows the k values calculated using Eq. (6). This expression reproduces the full radiative transfer sensitivity simulations with a root mean squared error (RMSE) of 0.004 and a coefficient of determination (r^2) of 0.99. Equation (6) does not apply for BrC/POC fractions less than 0.4 since they do not reproduce the absorption observed by OMI. We emphasize that multiple choices of k and BrC/POC will yield the same TOA radiance and UVAI. The effects on tropospheric OH concentrations and radiative forcing remain unaffected as BrC/POC and effective k vary together, since the distribution of scattering and absorption remains the same.

Table 5 contains our derived imaginary parts of the refractive index for BrC/POC fractions of 0.5 and 1.0.. Table 5 also contains effective k values derived for an organic carbon density of 1.8 g cm^{-3} which has been assumed in prior studies of BrC. The range of values for k covered by varying the BrC/POC fraction encompasses the range of values for BrC found in the literature (Chen and Bond, 2010; Feng et al., 2013; Kirchstetter et al., 2004; Lin et al., 2014; Sun et al., 2007; Wang et al., 2014; Zhang et al., 2013; Zhong and Jang, 2014). The four columns with BrC yield identical wavelength dependent global distributions of scattering and absorption that in turn yield the same UVAI, OH, and DRE.

The columns with effective *k* values for BrC/POC fraction of unity offer the convenience of representing the effective absorption by BrC without needing to assume an arbitrary BrC/POC fraction, or to introduce a separate BrC tracer. The effective *k* values for unity BrC/POC fraction can be thought of as the effective imaginary refractive index for an internal mixture of BrC and colorless POC.

Evidence for the existence of brown secondary organic carbon (Br-SOA) also exists. The majority of Br-SOA is from anthropogenic sources (Jo et al., 2015; Liu et al., 2013, 2014; Zhang et al., 2013), while SOA formed from biogenic carbon is largely non-absorbing (Flores et al., 2014; Liu et al., 2014). On a global scale it is estimated that the majority of SOA is formed from biogenic carbon (Hallquist et al., 2009; Lack et al., 2004; Tsigaridis and Kanakidou, 2003). Therefore we treat SOA as non-absorbing. We tested this approach in a sensitivity study with the standard SOA mechanism in GEOS-Chem v9-01-03 (Henze and Seinfeld, 2006; Henze et al., 2008; Liao et al., 2007) by assigning 100% anthropogenic SOA as brown, and found that the change in UVAI was negligible (less than 0.1). Alternative SOA implementations (e.g. as used in Jo et al., 2015) may have a larger effect.

4.3 Simulation including brown carbon

Figure 4 shows the monthly mean UVAI values for the simulation including brown carbon for the months of January, April, July, and September of 2007. The simulated absorption features including BrC are much more consistent than the base case simulation at reproducing the OMI UVAI over biomass burning regions (Figure 2). The simulated UVAI in the four biomass burning regions now ranges from 0.5-3. As summarized in Table 3, the correlation coefficients between the simulated and OMI UVAI for the four biomass burning regions now range from 0.57-0.68, with mean biases of -0.22 to +0.33.

The simulated UVAI using global mean *k* values underestimates the OMI observations for the West Africa and southern Africa regions, but overestimates observations in the South American region. We tested how *k* would need to change to explain the regional UVAI bias if *k* were the only error source. We find that these regional biases could be eliminated by changing *k* at 350 nm by +2% over West Africa, by +10% over southern Africa, and by -30% over South America. The presence of more absorbing BrC over West and southern Africa where savannah fires dominate, and less absorbing BrC over the South America region where forest fires dominate,

is consistent with work by Saleh et al. (2014) that found the absorptivity of BrC from biomass burning is greater for flaming fires associated with burning grasslands than for smouldering fires associated with burning forest.

The absorption in the West and southern Africa cases appears to be concentrated closer to the source for the simulated values (Figure 4) compared to the OMI values (Figure 1), which show an even distribution of UVAI values away from the source. By contrast, the absorption in the South American region appears to be distributed farther from the source in the simulation than in the OMI observations. Evidence exists of atmospheric photochemical loss and evaporation of brown carbon that causes it to become less absorbing over a lifetime of less than a day (Forrister et al., 2015; Zhong and Jang, 2014). Representing these processes would improve the simulation in the South American region but degrade the simulation in the West Africa and southern Africa regions. Regional treatment of BrC loss processes may be warranted in future work. The current implementation offers our best representation of the effective BrC absorption at the global scale.

Table 6 shows the calculated AAE values for biomass burning aerosol (i.e. black carbon + organic carbon aerosol) from our simulations for comparison with the literature values in Table 1. Large biases are apparent for the base case simulation without BrC. We evaluate the case 2 simulation including BrC in detail. For the 350-400 nm wavelength region our mean AAE value of 2.8 ± 0.22 for the four biomass burning regions is within the recommended values of 2.5-3.0 by Jethva and Torres (2011). In the 350-700 nm range our mean AAE of 2.2 ± 0.17 is close to the value of 1.9 from Kirchstetter and Thatcher (2012). The slight positive bias could arise from the fact that Kirchstetter and Thatcher (2012) took their absorption measurements from wood smoke emitted from houses in rural California during the winter, which have different conditions than the tropical open burning considered here. We obtain a mean AAE value of 1.7 ± 0.15 for the 300-1000 nm range, which falls within the literature values of 1.1 to 2. For the 450-550 nm wavelength region, we obtain a mean AAE value of 2.5 ± 0.14, which is biased high compared to the values from Corr et al. (2012) extracted from an examination of biomass burning plumes in North-Central Canada, where burn conditions differ from the mostly tropical regions considered in our analysis. Over the 400-700 nm region we obtain a mean AAE of 2.1 ± 0.15, falling within the range of the literature values (1.3-2.1). In the 400-1000 nm region, we obtain a mean AAE value of 1.3 ± 0.005, which is at the low end of the literature values (1.3-1.7). The overall consistency between

observed and simulated AAE provides a measure of confidence in spectral dependence of aerosol optical properties from the UV to the IR. We now examine the implications of this absorption for OH and DRE.

5. Analysis of the effect of absorption by BrC on OH concentrations in GEOS-Chem

The strong absorption in the UV by brown carbon aerosol decreases photolysis frequencies, which has implications for ozone photolysis and OH production. Here we examine the effect of the added absorption by BrC on the $O^3 \rightarrow O(^1D)$ photolysis frequency, $J(O(^1D))$, and tropospheric OH concentrations.

Figure 5 shows the percent differences in lower tropospheric OH concentrations between the GEOS-Chem simulation including absorbing brown carbon versus the base case simulation. The most significant decreases correspond with the major biomass burning regions. The addition of BrC decreases OH concentrations by up to 30% over the South American biomass burning region in September and up to 20% over the southern Africa biomass burning region in July. OH concentrations decrease by up to 15% over West Africa in January and southern Africa in September, with decreases of up to 5% over North America in July, South America in July, and South Asia in January, April, and September. The spatial and seasonal pattern of $J(O^1(D))$ differences closely reproduces the changes in OH ($r^2 = 0.85$) (not shown).

Methyl chloroform observations provide a valuable constraint on global OH (Prather et al., 2012; Spivakovsky et al., 2000). The addition of BrC to the GEOS-Chem simulation reduces global mean tropospheric OH concentrations. The reduction in global mean OH concentrations increases the methyl chloroform lifetime to tropospheric OH from 5.62 years to 5.68 years. This change is noteworthy given the buffered nature of OH. This change reduces the bias with observations giving a methyl chloroform lifetime of 6.0 (+0.5, -0.4) years (Prinn et al., 2005).

6. Radiative impact of brown carbon

We calculate the direct radiative effect (DRE) of including absorbing BrC relative to that of the base case simulation. We use GEOS-Chem coupled with the radiative transfer model RRTMG (Iacono et al., 2008), a configuration known as GC-RT, that is described in Heald et al. (2014). GC-RT calculates both the longwave (LW) and shortwave (SW) instantaneous total radiative fluxes as well as the flux differences due to a specific constituent of the atmosphere (e.g.

organic aerosol). The DRE is calculated by adding the LW and SW flux differences determined through perturbation of the constituent of interest. Our GC-RT simulations use version 10.1 of GEOS-Chem with the same aerosol emissions described in section 3 (e.g. GFED3 open fire emissions). We calculate the DRE of absorption by BrC as the difference in the DRE of organic aerosol when including BrC (Case 2) minus the DRE of organic aerosol in the base case. We focus on the DRE rather than the DRF to avoid ambiguity in preindustrial BrC.

Figure 6 shows all-sky DRE values for 2007. The top two panels are the DRE values for organic aerosol from the case 2 simulation including BrC. The overall DRE of organic aerosol including BrC is negative, with the largest effects over major biomass burning regions. The bottom two panels show the DRE for absorption by BrC, calculated as the difference between the DRE of organic aerosol for the case 2 simulation including BrC minus the base case simulation. At the surface BrC absorption reduces the DRE by -1.5 Wm^{-2} over South America and southern Africa, and by -0.5 to -0.25 Wm^{-2} over South Asia, North America, West Africa, Australia, and Europe. At TOA, BrC absorption increases the DRE by up to 0.3 Wm^{-2} over South America and southern Africa, and by 0.05 to 0.15 Wm^{-2} over broad regions. This overall cooling effect at the surface and warming effect on the atmosphere are consistent with previous work (e.g. Chen and Bond, 2010).

Table 7 contains LW and SW global annual mean flux differences as well as the resulting DRE values for both organic aerosol and brown carbon absorption. The values for organic aerosol are from the base case simulation assuming weakly absorbing organic carbon and the case 2 simulation including BrC, while the values for BrC absorption are calculated as their difference. Absorption by BrC has a mean all-sky DRE at TOA of +0.03 W m^{-2} and at the surface of -0.08 W m^{-2}.

Our findings are at the lower end of the range of values from other studies that estimate the DRE of BrC absorption. Feng et al. (2013) introduce absorption by BrC based on the optical properties from Kirchstetter et al. (2004) and Chen and Bond (2010) into a global model, and calculate an all-sky TOA DRE for BrC absorption of +0.04 to +0.11 W m^{-2}, and an all-sky surface DRE for BrC absorption of -0.06 to -0.14 W m^{-2}. Chung et al. (2012) estimate BrC absorption by subtracting the absorption by BC and desert dust from total aerosol AAE values from AERONET to calculate an all-sky TOA DRE for organic aerosol when including BrC between -0.15 and +0.12 W m^{-2} and an all-sky surface DRE between -1.50 and -0.75 W m^{-2}. Arola et al. (2015) use

AERONET retrieved imaginary parts of the refractive index for brown carbon at 440, 670, 870, and 1020 nm to estimate over the Indo-Gangetic plain monthly all-sky TOA DRE values for organic aerosol including BrC absorption up to +0.5 W m^{-2} in spring and as low as -1 W m^{-2} in the winter.

7. Conclusion

We interpret OMI observations of the Ultraviolet Aerosol Index (UVAI), which provides a measure of absorbing aerosols, by developing a simulation of the UVAI using the vector radiative transfer model VLIDORT coupled with GEOS-Chem aerosol fields. The base case simulation without brown carbon (BrC) well represents the observed UVAI in most of the world but significantly underestimates the absorption in biomass burning regions. We apply the OMI UVAI to estimate absorption by BrC. This approach exploits the strong absorption by BrC at ultraviolet wavelengths and its effect on top of atmosphere (TOA) radiance. We express the imaginary part of the refractive index of BrC that is required to obtain near-identical TOA radiance values as a function of the fraction of primary organic carbon that is brown. This effective refractive index of BrC provides a measure of the degree of browness needed to represent the complex processes (e.g. burn conditions, photochemical loss) affecting global BrC and in turn the UVAI. This effective refractive index of BrC eliminates the need to know the BrC/POC ratio to model the radiative effects of BrC. Rather, an effective refractive index can be chosen (eq. 6) to represent an internal mixture of BrC and colorless POC.

The simulation including absorbing BrC is much more consistent than the base case at reproducing the OMI UVAI over biomass burning regions. The mean bias between simulated and OMI UVAI values is reduced from -0.57 to -0.09 over West Africa in January, from -0.32 to +0.0002 over South Asia in April, from -0.97 to -0.22 over southern Africa in July, and from -0.50 to +0.33 over South America in September. The updated optical properties for BrC result in AAE values for biomass burning aerosol ranging from 2.9 in the UV to 1.3 across the UV-Near IR, which are broadly consistent with field observations.

We apply this constraint on ultraviolet absorption to examine implications for the $O_3 \rightarrow O(^1D)$ photolysis frequency. We find that the inclusion of absorbing BrC into GEOS-Chem decreases $J(O(^1D))$ and lower tropospheric OH by up to 30% over South America in September, up to 20% over southern Africa in July, up to 15% over West Africa in January and southern Africa

in September, and up to 5% elsewhere. The decrease in global mean OH concentration in GEOS-Chem increases the methyl chloroform lifetime to tropospheric OH from 5.62 years to 5.68 years, reducing the bias with estimates from observations of 6.0 (+0.5, -0.4) years.

We calculate the direct radiative effect (DRE) of BrC using GEOS-Chem coupled with the radiative transfer model RRTMG (GC-RT). We obtain global annual mean all-sky TOA DRE values for BrC absorption of +0.03 Wm^{-2} and values of -0.08 Wm^{-2} at the surface. Regional changes of up to +0.3 W m^{-2} at TOA and down to -1.5 W m^{-2} at the surface are found over major biomass burning regions. Our results are within the range of prior estimates of DRE for BrC absorption.

Ample opportunities exist to further develop the simulations of BrC and more generally of the UVAI. These opportunities include explicitly accounting for the range of processes affecting BrC such as burn conditions, photochemical loss, secondary production, as well as regional treatment of BrC. An explicit simulation of BrC (e.g. Jo et al. (2015)) would facilitate these developments. Interpretation of the long observational record of the UVAI from 1979 to the present should offer constraints on trends in aerosol composition, ultraviolet absorption, and radiative effects. The forthcoming TROPOMI instrument and geostationary constellation (e.g. TEMPO, Sentinel-4, and GEMS) will offer UVAI observations at 5-20 times higher spatial resolution, as well as information on diurnal variation, both of which may offer additional constraints on BrC evolution.

Acknowledgements: This work was supported by the Natural Science and Engineering Research Council of Canada. Computational facilities were provided in part by the Atlantic Computational Excellence Network consortium of Compute Canada. We thank Farhan Khan for assistance during the early stages of this work.

References

Aiken, A. C., DeCarlo, P. F., Kroll, J. H., Worsnop, D. R., Huffman, J. A., Docherty, K. S., Ulbrich, I. M., Mohr, C., Kimmel, J. R., Sueper, D., Sun, Y., Zhang, Q., Trimborn, A., Northway, M., Ziemann, P. J., Canagaratna, M. R., Onasch, T. B., Alfarra, M. R., Prevot, A. S. H., Dommen, J., Duplissy, J., Metzger, A., Baltensperger, U. and Jimenez, J. L.: O/C and OM/OC Ratios of Primary, Secondary, and Ambient Organic Aerosols with High-Resolution Time-of-Flight Aerosol Mass Spectrometry, Environ. Sci. Technol., 42(12), 4478–4485, doi:10.1021/es703009q, 2008.

Andreae, M. O. and Gelencsér, A.: Black carbon or brown carbon? The nature of light-absorbing carbonaceous aerosols, Atmos. Chem. Phys., 6(10), 3131–3148, doi:10.5194/acp-6-3131-2006, 2006.

Arola, A., Schuster, G., Myhre, G., Kazadzis, S., Dey, S. and Tripathi, S. N.: Inferring absorbing organic carbon content from AERONET data, Atmos. Chem. Phys., 11(1), 215–225, doi:10.5194/acp-11-215-2011, 2011.

Arola, A., Schuster, G. L., Pitkänen, M. R. A., Dubovik, O., Kokkola, H., Lindfors, A. V., Mielonen, T., Raatikainen, T., Romakkaniemi, S., Tripathi, S. N. and Lihavainen, H.: Measurement-based direct radiative effect by brown carbon over Indo-Gangetic Plain, Atmos. Chem. Phys. Discuss., 15(15), 21583–21606, doi:10.5194/acpd-15-21583-2015, 2015.

Bergstrom, R. W., Russell, P. B. and Hignett, P.: Wavelength Dependence of the Absorption of Black Carbon Particles: Predictions and Results from the TARFOX Experiment and Implications for the Aerosol Single Scattering Albedo, J. Atmos. Sci., 59(3), 567–577, doi:10.1175/1520-0469(2002)059<0567:WDOTAO>2.0.CO;2, 2002.

Bergstrom, R. W., Pilewskie, P., Russell, P. B., Redemann, J., Bond, T. C., Quinn, P. K. and Sierau, B.: Spectral absorption properties of atmospheric aerosols, Atmos. Chem. Phys., 7(23), 5937–5943, doi:10.5194/acp-7-5937-2007, 2007.

Bey, I., Jacob, D. J., Yantosca, R. M., Logan, J. A., Field, B. D., Fiore, A. M., Li, Q., Liu, H. Y., Mickley, L. J. and Schultz, M. G.: Global modeling of tropospheric chemistry with assimilated meteorology: Model description and evaluation, J. Geophys. Res., 106(D19), 23073, doi:10.1029/2001JD000807, 2001.

Bond, T. C.: Spectral dependence of visible light absorption by carbonaceous particles emitted from coal combustion, Geophys. Res. Lett., 28(21), 4075–4078, doi:10.1029/2001GL013652, 2001.

Bond, T. C. and Bergstrom, R. W.: Light Absorption by Carbonaceous Particles: An Investigative Review, Aerosol Sci. Technol., 40(1), 27–67, doi:10.1080/02786820500421521, 2006.

Bond, T. C., Bhardwaj, E., Dong, R., Jogani, R., Jung, S., Roden, C., Streets, D. G. and Trautmann, N. M.: Historical emissions of black and organic carbon aerosol from energy-related combustion, 1850-2000, Global Biogeochem. Cycles, 21(2), GB2018, doi:10.1029/2006GB002840, 2007.

Bond, T. C., Doherty, S. J., Fahey, D. W., Forster, P. M., Berntsen, T., DeAngelo, B. J., Flanner, M. G., Ghan, S., Kärcher, B., Koch, D., Kinne, S., Kondo, Y., Quinn, P. K., Sarofim, M. C., Schultz, M. G., Schulz, M., Venkataraman, C., Zhang, H., Zhang, S., Bellouin, N., Guttikunda,

S. K., Hopke, P. K., Jacobson, M. Z., Kaiser, J. W., Klimont, Z., Lohmann, U., Schwarz, J. P., Shindell, D., Storelvmo, T., Warren, S. G. and Zender, C. S.: Bounding the role of black carbon in the climate system: A scientific assessment, J. Geophys. Res. Atmos., 118(11), 5380–5552, doi:10.1002/jgrd.50171, 2013.

Buchard, V., da Silva, A. M., Colarco, P. R., Darmenov, A., Randles, C. A., Govindaraju, R., Torres, O., Campbell, J. and Spurr, R.: Using the OMI aerosol index and absorption aerosol optical depth to evaluate the NASA MERRA Aerosol Reanalysis, Atmos. Chem. Phys., 15(10), 5743–5760, doi:10.5194/acp-15-5743-2015, 2015.

Canagaratna, M. R., Jimenez, J. L., Kroll, J. H., Chen, Q., Kessler, S. H., Massoli, P., Hildebrandt Ruiz, L., Fortner, E., Williams, L. R., Wilson, K. R., Surratt, J. D., Donahue, N. M., Jayne, J. T. and Worsnop, D. R.: Elemental ratio measurements of organic compounds using aerosol mass spectrometry: characterization, improved calibration, and implications, Atmos. Chem. Phys., 15(1), 253–272, doi:10.5194/acp-15-253-2015, 2015.

Chen, Y. and Bond, T. C.: Light absorption by organic carbon from wood combustion, Atmos. Chem. Phys., 10(4), 1773–1787, doi:10.5194/acp-10-1773-2010, 2010.

Chung, C. E., Ramanathan, V. and Decremer, D.: Observationally constrained estimates of carbonaceous aerosol radiative forcing., Proc. Natl. Acad. Sci. U. S. A., 109(29), 11624–9, doi:10.1073/pnas.1203707109, 2012.

Clarke, A., McNaughton, C., Kapustin, V., Shinozuka, Y., Howell, S., Dibb, J., Zhou, J., Anderson, B. E., Brekhovskikh, V., Turner, H. and Pinkerton, M.: Biomass burning and pollution aerosol over North America: Organic components and their influence on spectral optical properties and humidification response, J. Geophys. Res. Atmos., 112(12), 1–13, doi:10.1029/2006JD007777, 2007.

Corr, C. A., Hall, S. R., Ullmann, K., Anderson, B. E., Beyersdorf, A. J., Thornhill, K. L., Cubison, M. J., Jimenez, J. L., Wisthaler, A. and Dibb, J. E.: Spectral absorption of biomass burning aerosol determined from retrieved single scattering albedo during ARCTAS, Atmos. Chem. Phys., 12(21), 10505–10518, doi:10.5194/acp-12-10505-2012, 2012.

Dave, J. V: Effect of Aerosols on the Estimation of Total Ozone in an Atmospheric Column from the Measurements of Its Ultraviolet Radiance, J. Atmos. Sci., 35(5), 899–911, doi:10.1175/1520-0469(1978)035<0899:EOAOTE>2.0.CO;2, 1978.

Dickerson, R. R., Kondragunta, S., Stenchikov, G., Civerolo, K. L., Doddridge, B. G. and Holben, B. N.: The impact of aerosols on solar ultraviolet radiation and photochemical smog., Science, 278(5339), 827–830, doi:10.1126/science.278.5339.827, 1997.

van Donkelaar, A., Martin, R. V., Leaitch, W. R., Macdonald, A. M., Walker, T. W., Streets, D. G., Zhang, Q., Dunlea, E. J., Jimenez, J. L., Dibb, J. E., Huey, L. G., Weber, R. and Andreae, M. O.: Analysis of aircraft and satellite measurements from the Intercontinental Chemical Transport Experiment (INTEX-B) to quantify long-range transport of East Asian sulfur to Canada, Atmos. Chem. Phys., 8(11), 2999–3014, doi:10.5194/acp-8-2999-2008, 2008.

Drury, E., Jacob, D. J., Spurr, R. J. D., Wang, J., Shinozuka, Y., Anderson, B. E., Clarke, A. D., Dibb, J., McNaughton, C. and Weber, R.: Synthesis of satellite (MODIS), aircraft (ICARTT), and surface (IMPROVE, EPA-AQS, AERONET) aerosol observations over eastern North America to improve MODIS aerosol retrievals and constrain surface aerosol concentrations and sources, J. Geophys. Res., 115(D14), D14204, doi:10.1029/2009JD012629, 2010.

569 Duplissy, J., DeCarlo, P. F., Dommen, J., Alfarra, M. R., Metzger, A., Barmpadimos, I., Prevot,
570 A. S. H., Weingartner, E., Tritscher, T., Gysel, M., Aiken, A. C., Jimenez, J. L., Canagaratna, M.
571 R., Worsnop, D. R., Collins, D. R., Tomlinson, J. and Baltensperger, U.: Relating hygroscopicity
572 and composition of organic aerosol particulate matter, Atmos. Chem. Phys., 11(3), 1155–1165,
573 doi:10.5194/acp-11-1155-2011, 2011.

574 Fairlie, D. J., Jacob, D. J. and Park, R. J.: The impact of transpacific transport of mineral dust in
575 the United States, Atmos. Environ., 41(6), 1251–1266, doi:10.1016/j.atmosenv.2006.09.048,
576 2007.

577 Feng, Y., Ramanathan, V. and Kotamarthi, V. R.: Brown carbon: A significant atmospheric
578 absorber of solar radiation, Atmos. Chem. Phys., 13(17), 8607–8621, doi:10.5194/acp-13-8607-
579 2013, 2013.

580 Flores, J. M., Washenfelder, R. A., Adler, G., Lee, H. J., Segev, L., Laskin, J., Laskin, A.,
581 Nizkorodov, S. A., Brown, S. S. and Rudich, Y.: Complex refractive indices in the near-
582 ultraviolet spectral region of biogenic secondary organic aerosol aged with ammonia., Phys.
583 Chem. Chem. Phys., 16(22), 10629–42, doi:10.1039/c4cp01009d, 2014.

584 Forrister, H., Liu, J., Scheuer, E., Dibb, J., Ziemba, L., Thornhill, K. L., Anderson, B., Diskin,
585 G., Perring, A. E., Schwarz, J. P., Campuzano-Jost, P., Day, D. A., Palm, B. B., Jimenez, J. L.,
586 Nenes, A. and Weber, R. J.: Evolution of brown carbon in wildfire plumes, Geophys. Res. Lett.,
587 42(11), 4623–4630, doi:10.1002/2015GL063897, 2015.

588 Fountoukis, C. and Nenes, A.: ISORROPIA II: a computationally efficient thermodynamic
589 equilibrium model for K^+–Ca^{2+}–Mg^{2+}–NH_4^+–Na^+–SO_4^{2-}–NO_3^-–Cl^-–H_2O aero, Atmos. Chem.
590 Phys., 7(17), 4639–4659, doi:10.5194/acp-7-4639-2007, 2007.

591 Hallquist, M., Wenger, J. C., Baltensperger, U., Rudich, Y., Simpson, D., Claeys, M., Dommen,
592 J., Donahue, N. M., George, C., Goldstein, A. H., Hamilton, J. F., Herrmann, H., Hoffmann, T.,
593 Iinuma, Y., Jang, M., Jenkin, M. E., Jimenez, J. L., Kiendler-Scharr, A., Maenhaut, W.,
594 McFiggans, G., Mentel, T. F., Monod, A., Prévôt, A. S. H., Seinfeld, J. H., Surratt, J. D.,
595 Szmigielski, R. and Wildt, J.: The formation, properties and impact of secondary organic aerosol:
596 current and emerging issues, Atmos. Chem. Phys., 9(14), 5155–5236, doi:10.5194/acp-9-5155-
597 2009, 2009.

598 Heald, C. L., Ridley, D. A., Kroll, J. H., Barrett, S. R. H., Cady-Pereira, K. E., Alvarado, M. J.
599 and Holmes, C. D.: Contrasting the direct radiative effect and direct radiative forcing of aerosols,
600 Atmos. Chem. Phys., 14(11), 5513–5527, doi:10.5194/acp-14-5513-2014, 2014.

601 Henze, D. K. and Seinfeld, J. H.: Global secondary organic aerosol from isoprene oxidation,
602 Geophys. Res. Lett., 33, L09812, 2006.

603 Henze, D. K., Seinfeld, J. H., Ng, N. L., Kroll, J. H., Fu, T.-M., Jacob, D. J. and Heald, C. L.:
604 Global modeling of secondary organic aerosol formation from aromatic hydrocarbons: high- vs.
605 low-yield pathways, Atmos. Chem. Phys., 8(9), 2405–2420, doi:10.5194/acp-8-2405-2008, 2008.

606 Herman, J. R., Bhartia, P. K., Torres, O., Hsu, C., Seftor, C. and Celarier, E.: Global distribution
607 of UV-absorbing aerosols from Nimbus 7/TOMS data, J. Geophys. Res., 102(D14), 16911,
608 doi:10.1029/96JD03680, 1997.

609 Iacono, M. J., Delamere, J. S., Mlawer, E. J., Shephard, M. W., Clough, S. A. and Collins, W.
610 D.: Radiative forcing by long-lived greenhouse gases: Calculations with the AER radiative

transfer models, J. Geophys. Res., 113(D13), D13103, doi:10.1029/2008JD009944, 2008.

IPCC: Climate Change 2014: Impacts, Adaptation, and Vulnerability. Part A: Global and Sectoral Aspects. Contribution of Working Group II to the Fifth Assessment Report of the Intergovernmental Panel on Climate Change [Field, C.B., V.R. Barros, D.J. Dokken, K.J., Cambridge University Press, Cambridge, United Kingdom and New York, NY, USA., 2014.

Jacobson, M. Z.: Studying the effects of aerosols on vertical photolysis rate coefficient and temperature profiles over an urban airshed, J. Geophys. Res., 103(D9), 10593, doi:10.1029/98JD00287, 1998.

Jaeglé, L., Quinn, P. K., Bates, T. S., Alexander, B. and Lin, J.-T.: Global distribution of sea salt aerosols: new constraints from in situ and remote sensing observations, Atmos. Chem. Phys., 11(7), 3137–3157, doi:10.5194/acp-11-3137-2011, 2011.

Jethva, H. and Torres, O.: Satellite-based evidence of wavelength-dependent aerosol absorption in biomass burning smoke inferred from Ozone Monitoring Instrument, Atmos. Chem. Phys., 11(20), 10541–10551, doi:10.5194/acp-11-10541-2011, 2011.

Jo, D. S., Park, R. J., Lee, S., Kim, S.-W. and Zhang, X.: A global simulation of brown carbon: implications for photochemistry and direct radiative effect, Atmos. Chem. Phys. Discuss., 15(19), 27805–27852, doi:10.5194/acpd-15-27805-2015, 2015.

Kirchstetter, T. W. and Thatcher, T. L.: Contribution of organic carbon to wood smoke particulate matter absorption of solar radiation, Atmos. Chem. Phys., 12(14), 6067–6072, doi:10.5194/acp-12-6067-2012, 2012.

Kirchstetter, T. W., Novakov, T. and Hobbs, P. V.: Evidence that the spectral dependence of light absorption by aerosols is affected by organic carbon, J. Geophys. Res. D Atmos., 109(21), D21208, doi:10.1029/2004JD004999, 2004.

Koepke, P., Hess, M., Schult, I. and Shettle, E. P.: Global Aerosol Dataset, report, Max-Planck Inst. fur Meteorol., Hamburg, Germany., 1997.

Kuhns, H., Knipping, E. M. and Vukovich, J. M.: Development of a United States–Mexico Emissions Inventory for the Big Bend Regional Aerosol and Visibility Observational (BRAVO) Study, J. Air Waste Manage. Assoc., 55(5), 677–692, doi:10.1080/10473289.2005.10464648, 2005.

Kuwata, M., Zorn, S. R. and Martin, S. T.: Using elemental ratios to predict the density of organic material composed of carbon, hydrogen, and oxygen., Environ. Sci. Technol., 46(2), 787–94, doi:10.1021/es202525q, 2012.

Lack, D. A. and Langridge, J. M.: On the attribution of black and brown carbon light absorption using the Ångström exponent, Atmos. Chem. Phys., 13(20), 10535–10543, doi:10.5194/acp-13-10535-2013, 2013.

Lack, D. A., Tie, X. X., Bofinger, N. D., Wiegand, A. N. and Madronich, S.: Seasonal variability of secondary organic aerosol: A global modeling study, J. Geophys. Res., 109(D3), D03203, doi:10.1029/2003JD003418, 2004.

Lee, C., Martin, R. V., van Donkelaar, A., O'Byrne, G., Krotkov, N., Richter, A., Huey, L. G. and Holloway, J. S.: Retrieval of vertical columns of sulfur dioxide from SCIAMACHY and OMI: Air mass factor algorithm development, validation, and error analysis, J. Geophys. Res., 114(D22), D22303, doi:10.1029/2009JD012123, 2009.

Leibensperger, E. M., Mickley, L. J., Jacob, D. J., Chen, W.-T., Seinfeld, J. H., Nenes, A., Adams, P. J., Streets, D. G., Kumar, N. and Rind, D.: Climatic effects of 1950–2050 changes in US anthropogenic aerosols – Part 2: Climate response, Atmos. Chem. Phys., 12(7), 3349–3362, doi:10.5194/acp-12-3349-2012, 2012.

Liao, H., Adams, P. J., Chung, S. H., Seinfeld, J. H., Mickley, L. J. and Jacob, D. J.: Interactions between tropospheric chemistry and aerosols in a unified general circulation model, J. Geophys. Res., 108(D1), 4001, doi:10.1029/2001JD001260, 2003.

Liao, H., Henze, D. K., Seinfeld, J. H., Wu, S. and Mickley, L. J.: Biogenic secondary organic aerosol over the United States: Comparison of climatological simulations with observations, J. Geophys. Res., 112(D6), D06201, doi:10.1029/2006JD007813, 2007.

Lin, G., Penner, J. E., Flanner, M. G., Sillman, S., Xu, L. and Zhou, C.: Radiative forcing of organic aerosol in the atmosphere and on snow: Effects of SOA and brown carbon, J. Geophys. Res. Atmos., 119(12), 7453–7476, doi:10.1002/2013JD021186, 2014.

Liu, J., Bergin, M., Guo, H., King, L., Kotra, N., Edgerton, E. and Weber, R. J.: Size-resolved measurements of brown carbon in water and methanol extracts and estimates of their contribution to ambient fine-particle light absorption, Atmos. Chem. Phys., 13(24), 12389–12404, doi:10.5194/acp-13-12389-2013, 2013.

Liu, J., Scheuer, E., Dibb, J., Diskin, G. S., Ziemba, L. D., Thornhill, K. L., Anderson, B. E., Wisthaler, A., Mikoviny, T., Devi, J. J., Bergin, M., Perring, A. E., Markovic, M. Z., Schwarz, J. P., Campuzano-Jost, P., Day, D. A., Jimenez, J. L. and Weber, R. J.: Brown carbon aerosol in the North American continental troposphere: sources, abundance, and radiative forcing, Atmos. Chem. Phys., 15(14), 7841–7858, doi:10.5194/acp-15-7841-2015, 2015.

Liu, P. F., Abdelmalki, N., Hung, H.-M., Wang, Y., Brune, W. H. and Martin, S. T.: Ultraviolet and visible complex refractive indices of secondary organic material produced by photooxidation of the aromatic compounds toluene and *m*-Xylene, Atmos. Chem. Phys. Discuss., 14(14), 20585–20615, doi:10.5194/acpd-14-20585-2014, 2014.

Mao, J., Fan, S., Jacob, D. J. and Travis, K. R.: Radical loss in the atmosphere from Cu-Fe redox coupling in aerosols, Atmos. Chem. Phys., 13(2), 509–519, doi:10.5194/acp-13-509-2013, 2013.

Martin, R. V., Jacob, D. J., Yantosca, R. M., Chin, M. and Ginoux, P.: Global and regional decreases in tropospheric oxidants from photochemical effects of aerosols, J. Geophys. Res., 108(D3), 4097, doi:10.1029/2002JD002622, 2003.

Martins, J. V., Artaxo, P., Kaufman, Y. J., Castanho, A. D. and Remer, L. A.: Spectral absorption properties of aerosol particles from 350–2500nm, Geophys. Res. Lett., 36(13), 1–5, doi:10.1029/2009GL037435, 2009.

Mu, M., Randerson, J. T., van der Werf, G. R., Giglio, L., Kasibhatla, P., Morton, D., Collatz, G. J., DeFries, R. S., Hyer, E. J., Prins, E. M., Griffith, D. W. T., Wunch, D., Toon, G. C., Sherlock, V. and Wennberg, P. O.: Daily and 3-hourly variability in global fire emissions and consequences for atmospheric model predictions of carbon monoxide, J. Geophys. Res. Atmos., 116(D24), D24303, doi:10.1029/2011JD016245, 2011.

Naik, V., Voulgarakis, A., Fiore, A. M., Horowitz, L. W., Lamarque, J.-F., Lin, M., Prather, M. J., Young, P. J., Bergmann, D., Cameron-Smith, P. J., Cionni, I., Collins, W. J., Dalsøren, S. B., Doherty, R., Eyring, V., Faluvegi, G., Folberth, G. A., Josse, B., Lee, Y. H., MacKenzie, I. A.,

695 Nagashima, T., van Noije, T. P. C., Plummer, D. A., Righi, M., Rumbold, S. T., Skeie, R.,
696 Shindell, D. T., Stevenson, D. S., Strode, S., Sudo, K., Szopa, S. and Zeng, G.: Preindustrial to
697 present-day changes in tropospheric hydroxyl radical and methane lifetime from the
698 Atmospheric Chemistry and Climate Model Intercomparison Project (ACCMIP), Atmos. Chem.
699 Phys., 13(10), 5277–5298, doi:10.5194/acp-13-5277-2013, 2013.

700 Olivier, J. G. J., Van Aardenne, J. A., Dentener, F. J., Pagliari, V., Ganzeveld, L. N. and Peters,
701 J. A. H. W.: Recent trends in global greenhouse gas emissions:regional trends 1970–2000 and
702 spatial distributionof key sources in 2000, Environ. Sci., 2(2-3), 81–99,
703 doi:10.1080/15693430500400345, 2005.

704 Park, R. J., Jacob, D. J., Chin, M. and Martin, R. V.: Sources of carbonaceous aerosols over the
705 United States and implications for natural visibility, J. Geophys. Res., 108(D12), 4355,
706 doi:10.1029/2002JD003190, 2003.

707 Park, R. J., Jacob, D. J., Field, B. D., Yantosca, R. M. and Chin, M.: Natural and transboundary
708 pollution influences on sulfate-nitrate-ammonium aerosols in the United States: Implications for
709 policy, J. Geophys. Res., 109(D15), D15204, doi:10.1029/2003JD004473, 2004.

710 Park, R. J., Kim, M. J., Jeong, J. I., Youn, D. and Kim, S.: A contribution of brown carbon
711 aerosol to the aerosol light absorption and its radiative forcing in East Asia, Atmos. Environ.,
712 44(11), 1414–1421, doi:10.1016/j.atmosenv.2010.01.042, 2010.

713 Prather, M. J., Holmes, C. D. and Hsu, J.: Reactive greenhouse gas scenarios: Systematic
714 exploration of uncertainties and the role of atmospheric chemistry, Geophys. Res. Lett., 39(9),
715 L09803, doi:10.1029/2012GL051440, 2012.

716 Prinn, R. G., Huang, J., Weiss, R. F., Cunnold, D. M., Fraser, P. J., Simmonds, P. G.,
717 McCulloch, A., Harth, C., Reimann, S., Salameh, P., O'Doherty, S., Wang, R. H. J., Porter, L.
718 W., Miller, B. R. and Krummel, P. B.: Evidence for variability of atmospheric hydroxyl radicals
719 over the past quarter century, Geophys. Res. Lett., 32(7), L07809, doi:10.1029/2004GL022228,
720 2005.

721 Pye, H. O. T., Liao, H., Wu, S., Mickley, L. J., Jacob, D. J., Henze, D. K. and Seinfeld, J. H.:
722 Effect of changes in climate and emissions on future sulfate-nitrate-ammonium aerosol levels in
723 the United States, J. Geophys. Res., 114(D1), D01205, doi:10.1029/2008JD010701, 2009.

724 Ramanathan, V. and Carmichael, G.: Global and regional climate changes due to black carbon,
725 Nat. Geosci., 1(4), 221–227, doi:10.1038/ngeo156, 2008.

726 Ridley, D. A., Heald, C. L. and Ford, B.: North African dust export and deposition: A satellite
727 and model perspective, J. Geophys. Res., 117(D2), D02202, doi:10.1029/2011JD016794, 2012.

728 Rizzo, L. V., Correia, A. L., Artaxo, P., Procápio, A. S. and Andreae, M. O.: Spectral
729 dependence of aerosol light absorption over the Amazon Basin, Atmos. Chem. Phys., 11(17),
730 8899–8912, doi:10.5194/acp-11-8899-2011, 2011.

731 Russell, P. B., Bergstrom, R. W., Shinozuka, Y., Clarke, A. D., DeCarlo, P. F., Jimenez, J. L.,
732 Livingston, J. M., Redemann, J., Holben, B., Dubovik, O. and Strawa, A.: Absorption Angstrom
733 Exponent in AERONET and related data as an indicator of aerosol composition, Atmos. Chem.
734 Phys. Discuss., 9(5), 21785–21817, doi:10.5194/acpd-9-21785-2009, 2009.

735 Saleh, R., Robinson, E. S., Tkacik, D. S., Ahern, A. T., Liu, S., Aiken, A. C., Sullivan, R. C.,
736 Presto, A. A., Dubey, M. K., Yokelson, R. J., Donahue, N. M. and Robinson, A. L.: Brownness

737 of organics in aerosols from biomass burning linked to their black carbon content, Nat. Geosci.,
738 7(9), 647–650, doi:10.1038/ngeo2220, 2014.

739 Spivakovsky, C. M., Logan, J. A., Montzka, S. A., Balkanski, Y. J., Foreman-Fowler, M., Jones,
740 D. B. A., Horowitz, L. W., Fusco, A. C., Brenninkmeijer, C. A. M., Prather, M. J., Wofsy, S. C.
741 and McElroy, M. B.: Three-dimensional climatological distribution of tropospheric OH: Update
742 and evaluation, J. Geophys. Res., 105(D7), 8931, doi:10.1029/1999JD901006, 2000.

743 Spurr, R. J. D.: VLIDORT: A linearized pseudo-spherical vector discrete ordinate radiative
744 transfer code for forward model and retrieval studies in multilayer multiple scattering media, J.
745 Quant. Spectrosc. Radiat. Transf., 102(2), 316–342, doi:10.1016/j.jqsrt.2006.05.005, 2006.

746 Stier, P., Seinfeld, J. H., Kinne, S. and Boucher, O.: Aerosol absorption and radiative forcing,
747 Atmos. Chem. Phys., 7(19), 5237–5261, doi:10.5194/acp-7-5237-2007, 2007.

748 Sun, H., Biedermann, L. and Bond, T. C.: Color of brown carbon: A model for ultraviolet and
749 visible light absorption by organic carbon aerosol, Geophys. Res. Lett., 34(17), L17813,
750 doi:10.1029/2007GL029797, 2007.

751 Torres, O., Bhartia, P. K., Herman, J. R., Ahmad, Z. and Gleason, J.: Derivation of aerosol
752 properties from satellite measurements of backscattered ultraviolet radiation: Theoretical basis, J.
753 Geophys. Res., 103(D14), 17099, doi:10.1029/98JD00900, 1998.

754 Torres, O., Bhartia, P. K., Sinyuk, A., Welton, E. J. and Holben, B.: Total Ozone Mapping
755 Spectrometer measurements of aerosol absorption from space: Comparison to SAFARI 2000
756 ground-based observations, J. Geophys. Res., 110(D10), D10S18, doi:10.1029/2004JD004611,
757 2005.

758 Torres, O., Tanskanen, A., Veihelmann, B., Ahn, C., Braak, R., Bhartia, P. K., Veefkind, P. and
759 Levelt, P.: Aerosols and surface UV products from Ozone Monitoring Instrument observations:
760 An overview, J. Geophys. Res., 112(D24), D24S47, doi:10.1029/2007JD008809, 2007.

761 Torres, O., Ahn, C. and Chen, Z.: Improvements to the OMI near-UV aerosol algorithm using A-
762 train CALIOP and AIRS observations, Atmos. Meas. Tech., 6(11), 3257–3270, doi:10.5194/amt-
763 6-3257-2013, 2013.

764 Tsigaridis, K. and Kanakidou, M.: Global modelling of secondary organic aerosol in the
765 troposphere: a sensitivity analysis, Atmos. Chem. Phys., 3(5), 1849–1869, doi:10.5194/acp-3-
766 1849-2003, 2003.

767 Turpin, B. J. and Lim, H.-J.: Species Contributions to PM2.5 Mass Concentrations: Revisiting
768 Common Assumptions for Estimating Organic Mass, Aerosol Sci. Technol., 35(1), 602–610,
769 doi:10.1080/02786820119445, 2001.

770 Wang, X., Heald, C. L., Ridley, D. A., Schwarz, J. P., Spackman, J. R., Perring, A. E., Coe, H.,
771 Liu, D. and Clarke, A. D.: Exploiting simultaneous observational constraints on mass and
772 absorption to estimate the global direct radiative forcing of black carbon and brown carbon,
773 Atmos. Chem. Phys., 14(20), 10989–11010, doi:10.5194/acp-14-10989-2014, 2014.

774 Yang, M., Howell, S. G., Zhuang, J. and Huebert, B. J.: Attribution of aerosol light absorption to
775 black carbon, brown carbon, and dust in China- interpretations of atmospheric measurements
776 during EAST-AIRE, Atmos. Chem. Phys. Discuss., 8(3), 10913–10954, doi:10.5194/acpd-8-
777 10913-2008, 2008.

778 Yevich, R. and Logan, J. A.: An assessment of biofuel use and burning of agricultural waste in

the developing world, Global Biogeochem. Cycles, 17(4), 1095, doi:10.1029/2002GB001952, 2003.

Zhang, L., Jacob, D. J., Kopacz, M., Henze, D. K., Singh, K. and Jaffe, D. A.: Intercontinental source attribution of ozone pollution at western U.S. sites using an adjoint method, Geophys. Res. Lett., 36, L11810 [online] Available from: http://dash.harvard.edu/handle/1/3627131 (Accessed 9 May 2015), 2009.

Zhang, X., Lin, Y.-H., Surratt, J. D. and Weber, R. J.: Sources, composition and absorption Ångström exponent of light-absorbing organic components in aerosol extracts from the Los Angeles Basin., Environ. Sci. Technol., 47(8), 3685–93, doi:10.1021/es305047b, 2013.

Zhong, M. and Jang, M.: Dynamic light absorption of biomass-burning organic carbon photochemically aged under natural sunlight, Atmos. Chem. Phys., 14(3), 1517–1525, doi:10.5194/acp-14-1517-2014, 2014.

Tables and Figures

Table 1: Absorption Angstrom Exponent (AAE) values for biomass burning regions from the literature.

Wavelength (nm)	AAE value	Region	Reference
350-400 nm			
350-400	2.5-3.0	South America	Jethva and Torres, 2011
350-700 nm			
360-700	1.9	Rural California	Kirchstetter and Thatcher, 2012
450-550 nm			
470-532	1.9	North-central Canada	Corr et al. 2012
470-532	1.4	"	"
Mean ± SD* = 1.7 ± 0.35			
400-700 nm			
400-700	1.5-1.9	Laboratory	Schnaiter et al. 2005
440-670	1.8	Boreal Forest	Russell et al. 2010
440-670	1.3	Southern Africa	"
440-670	1.4	South America	"
440-670	1.6	Amazon	"
470-660	1.7	Arctic	Corr et al. 2012
470-660	1.3	Arctic	"
470-660	1.5	Outside Beijing	Yang et al. 2009
470-660	2.1	North America	Clarke et al. 2007
Mean ± SD = 1.6 ±0.26			
450-700 nm			
470-660	2.2	North America	Liu et al. 2015
300-1000 nm			
325-1000	1.1	Southern Africa	Bergstrom et al. 2007
325-1685	1.5	Southern Africa	"
330-1000	2	Southern Africa	Kirchstetter et al. 2004
370-950	1.5	Outside Beijing	Yang et al. 2009
Mean ± SD = 1.5 ± 0.37			
400-1000 nm			
440-870	1.6	Boreal Forest	Russell et al. 2010
440-870	1.3	Southern Africa	"
440-870	1.4	South America	"
440-870	1.4	Amazon	"
440-1020	1.5	Boreal Forest	"
440-1020	1.3	Southern Africa	"
440-1020	1.3	South America	"
440-1020	1.4	Amazon	"
450-950	1.7	Amazon	Rizzo et al. 2011
Mean ± SD = 1.4 ± 0.14			

***SD: standard deviation**

Table 2: Imaginary part of the refractive index (k) values for the base case with weakly absorbing "colorless" primary organic carbon.

Wavelength (nm)	Base Case
300	0.008
350	0.005
400	0.005
450	0.005
500	0.005
550	0.006

Table 3: Comparison of the simulated versus observed (OMI) UVAI values for the biomass burning regions in the months examined. The base case corresponds to a simulation without BrC, while Case 2 corresponds to a simulation including absorbing BrC.

			Mean	Base Case		Case 2 with BrC	
Region[d]	**n**[c]	**Month**	**OMI UVAI**	**r**[a]	**Mean Bias**[b]	**r**	**Mean Bias**
West Africa	381	January	1.25	0.48	-0.57	0.68	-0.09
South Asia	280	April	0.34	0.46	-0.32	0.66	+0.0002
Southern Africa	184	July	0.66	0.09	-0.97	0.63	-0.22
South America	230	September	0.30	0.40	-0.50	0.57	+0.33

[a] r: Pearson correlation coefficient
[b] Mean bias = simulated UVAI – observed UVAI
[c] n = number of GEOS-Chem grid boxes in region
[d] regions are defined in Figure 1

Table 4: The mean AOD values for each region from the GEOS-Chem (GC) base case simulation, the MISR instrument, and the MODIS Terra satellite instrument. The MODIS values are included for both the collection 6 Deep Blue and Dark Target algorithms.

	Mean AOD			
Region[a]	**GC**	**MISR**	**MODIS Deep Blue**	**MODIS Dark Target**
West Africa	0.42	0.42	0.45	0.51
South Asia	0.32	0.32	0.30	0.37
Southern Africa	0.19	0.19	0.13	0.24
South America	0.31	0.36	0.39	0.57

[a] regions are defined in Figure 1

887 **Table 5:** Imaginary part of the refractive index (k) values for brown carbon (not total organic carbon)
888 inferred for case 2. We include k values associated with multiple densities (ρ), and multiple fractions of
889 brown carbon to primary organic carbon (BrC/POC). All four columns for case 2 yield the same
890 absorption.

	Case 2 with BrC (ρ = 1.3 g cm^{-3})		Case 2 with BrC (ρ = 1.8 g cm^{-3})	
Wavelength (nm)	**BrC/POC = 0.50**	**BrC/POC = 1.0**	**BrC/POC = 0.50**	**BrC/POC=1.0**
300	0.11	0.051	0.16	0.071
350	0.077	0.037	0.11	0.051
400	0.052	0.025	0.073	0.035
450	0.035	0.014	0.049	0.019
500	0.023	0.009	0.032	0.013
550	0.015	0.007	0.021	0.010

891
892
893
894
895
896
897
898
899
900
901
902
903
904
905
906
907
908
909
910
911
912

Table 6: The Absorption Angstrom Exponent (AAE) values for major biomass burning regions and seasons obtained from the base case simulation without BrC and the case 2 simulation including absorbing BrC.

Wavelength (nm)	January (West Africa)	April (South Asia)	July (Southern Africa)	September (South America)	Mean ± SD*
Base Case					
350-400	1.2	1.2	1.2	1.2	1.2 ± 0.00
350-700	1.0	1.2	1.0	1.1	1.1 ± 0.09
450-550	0.8	1.1	0.7	1.0	0.9 ± 0.18
400-700	1.0	1.2	0.9	1.1	1.1 ± 0.13
450-700	1.0	1.1	0.9	1.0	1.0 ± 0.08
300-1000	0.9	1.1	0.9	0.9	0.9 ± 0.10
400-1000	0.7	0.9	0.7	0.7	0.8 ± 0.10
Case 2 with BrC					
350-400	2.9	2.5	3	2.9	2.8 ± 0.22
350-700	2.3	2	2.4	2.3	2.2 ± 0.17
450-550	2.5	2.3	2.6	2.6	2.5 ± 0.14
400-700	2.2	1.9	2.2	2.2	2.1 ± 0.15
450-700	1.9	1.7	1.9	1.9	1.8 ± 0.10
300-1000	1.8	1.6	1.8	1.8	1.7 ± 0.15
400-1000	1.3	1.3	1.3	1.3	1.3 ± 0.00

*SD: standard deviation

Table 7: Global annual mean LW and SW flux differences and resulting DRE values for 2007 at TOA and the surface. The values for organic aerosol are shown for both the base case simulation without BrC and the case 2 simulation including absorbing brown carbon. The DRE values for BrC absorption are calculated as the difference between the DRE of organic aerosol from case 2 minus the base case.

	Organic Aerosol		**BrC Absorption**
	Base Case	**Case 2**	**Case 2 – Base Case**
TOA DRE, Clear Sky (Wm^{-2})	-0.33	-0.31	+0.02
LW	+0.0026	+0.0028	
SW	-0.33	-0.31	
TOA DRE, All Sky (Wm^{-2})	-0.24	-0.21	+0.03
LW	+0.0020	+0.0021	
SW	-0.24	-0.21	
Surface DRE, Clear Sky (Wm^{-2})	-0.50	-0.60	-0.09
LW	+0.0061	+0.0067	
SW	-0.51	-0.61	
Surface DRE, All Sky (Wm^{-2})	-0.41	-0.49	-0.08
LW	+0.0051	+0.0056	
SW	-0.42	-0.5	

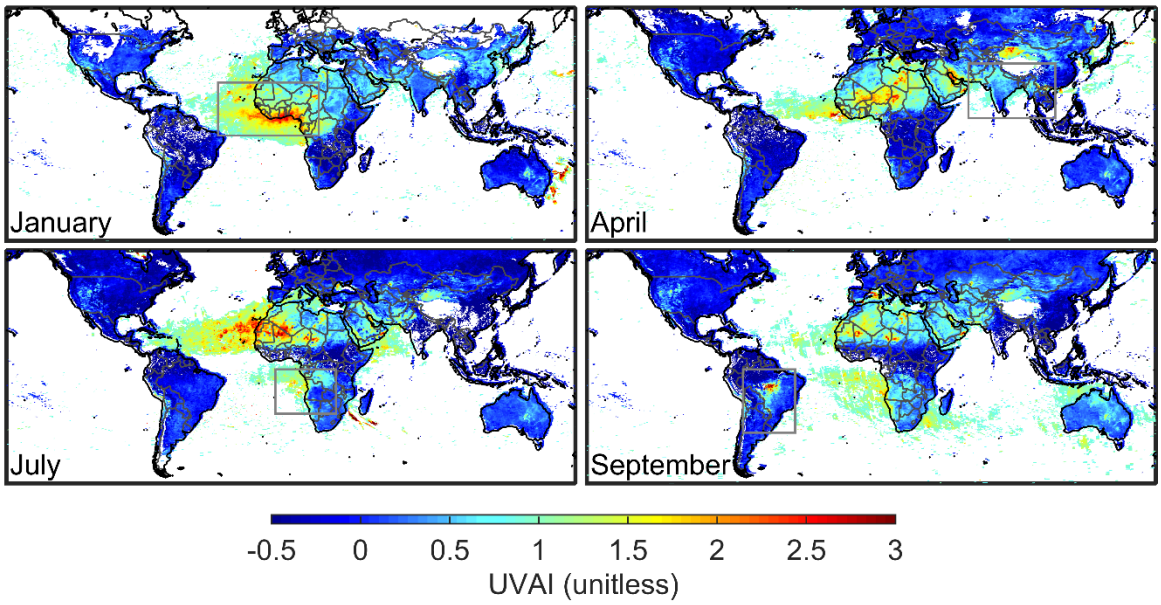

944

945 **Figure 1:** Monthly mean Ultraviolet Aerosol Index (UVAI) observations from the OMI satellite
946 instrument for 2007. White space indicates cloud or snow contamination. Grey boxes outline
947 regions examined in Tables 3 and 4.

948

949

950

951

952

953

954

955

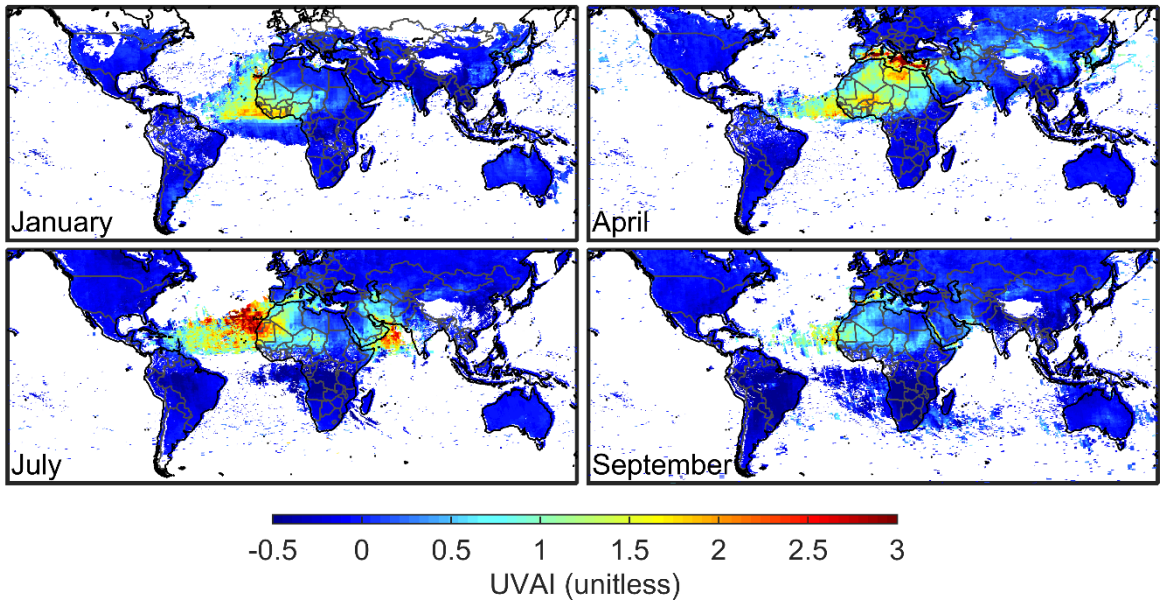

956

957 **Figure 2:** Monthly mean UVAI values for 2007 simulated for OMI observing conditions using the
958 vector radiative transfer model VLIDORT coupled with GEOS-Chem aerosol fields for the base
959 case without brown carbon (BrC). White indicates cloud or snow contamination.

960

961

962

963

964

965

966

967

968

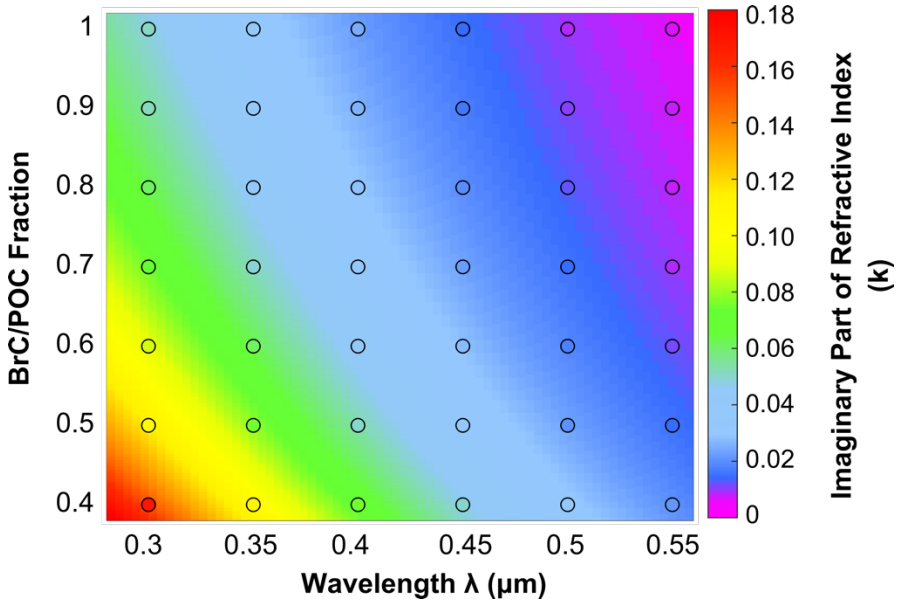

969

970 **Figure 3:** Imaginary part of the refractive index (*k*) values inferred for BrC as a function of
971 wavelength and of the assumed fraction of primary organic carbon that is brown (BrC/POC). The
972 background spectrum represents *k* values calculated using Eq. (6). The filled circles represent the
973 *k* values obtained from sensitivity simulations. An organic carbon density of 1.3 g cm^{-3} is assumed.

974

975

976

977

978

979

980

981

982

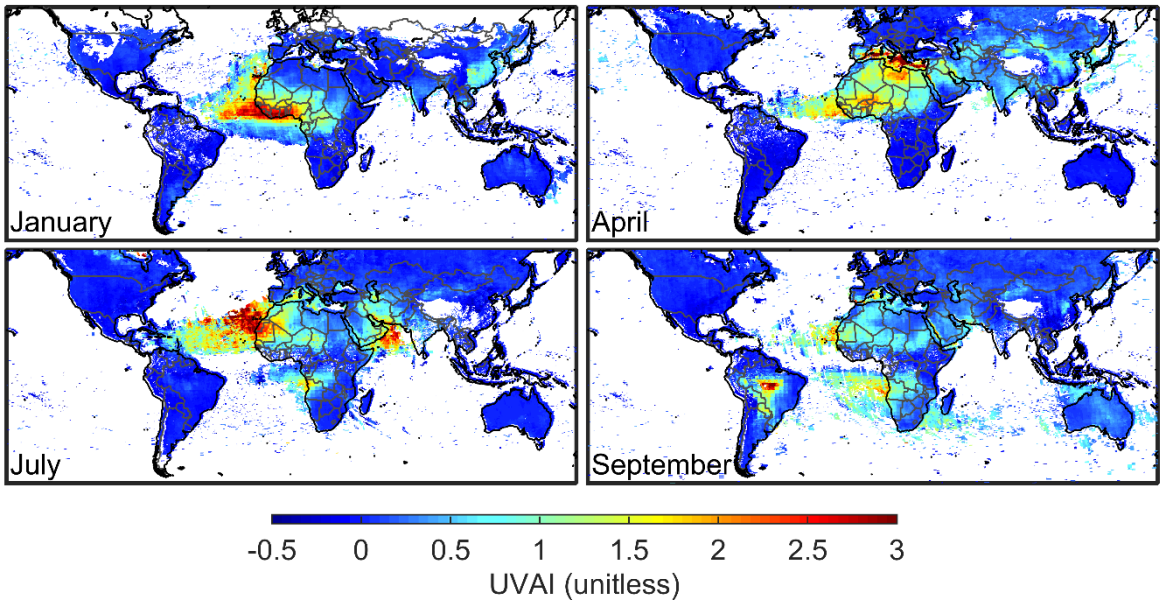

983

984 **Figure 4:** Monthly mean UVAI values for 2007 simulated for OMI observing conditions using the
985 vector radiative transfer model VLIDORT coupled with GEOS-Chem aerosol fields for case 2,
986 which assumes the presence of absorbing BrC aerosol. White indicates clouds or snow
987 contamination.

988

989

990

991

992

993

994

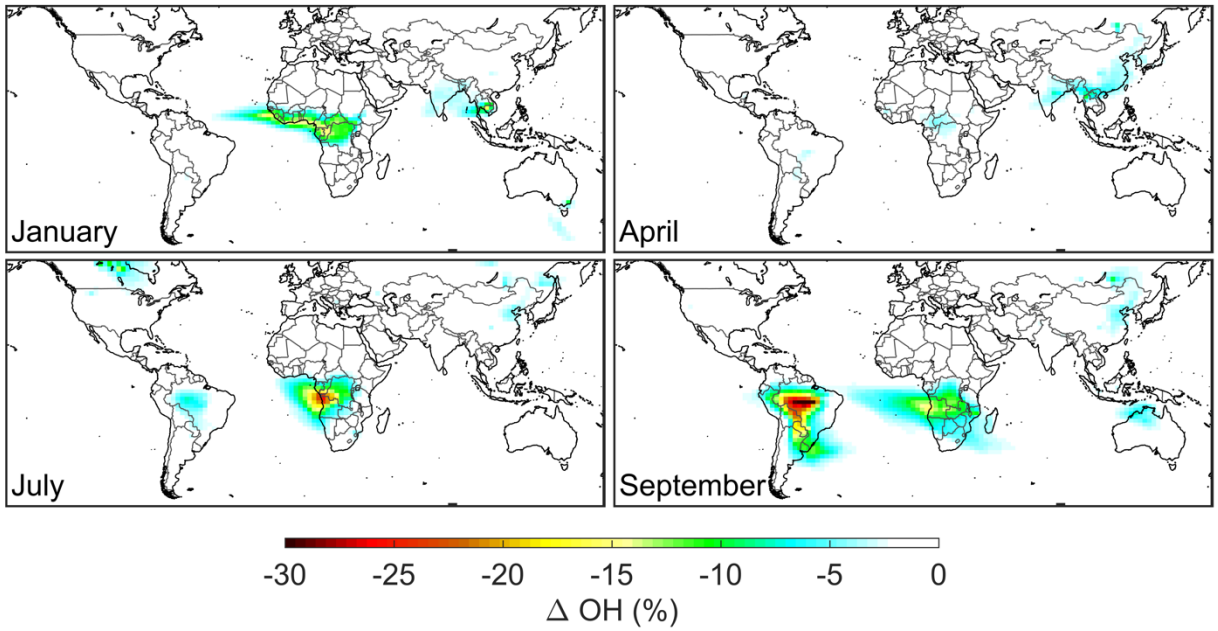

995

996 **Figure 5:** Percent difference between OH concentrations in the lower troposphere from a GEOS-
997 Chem simulation including absorbing BrC minus a simulation without BrC. The values are
998 monthly means for January, April, July, and September of 2007.

999

1000

1001

1002

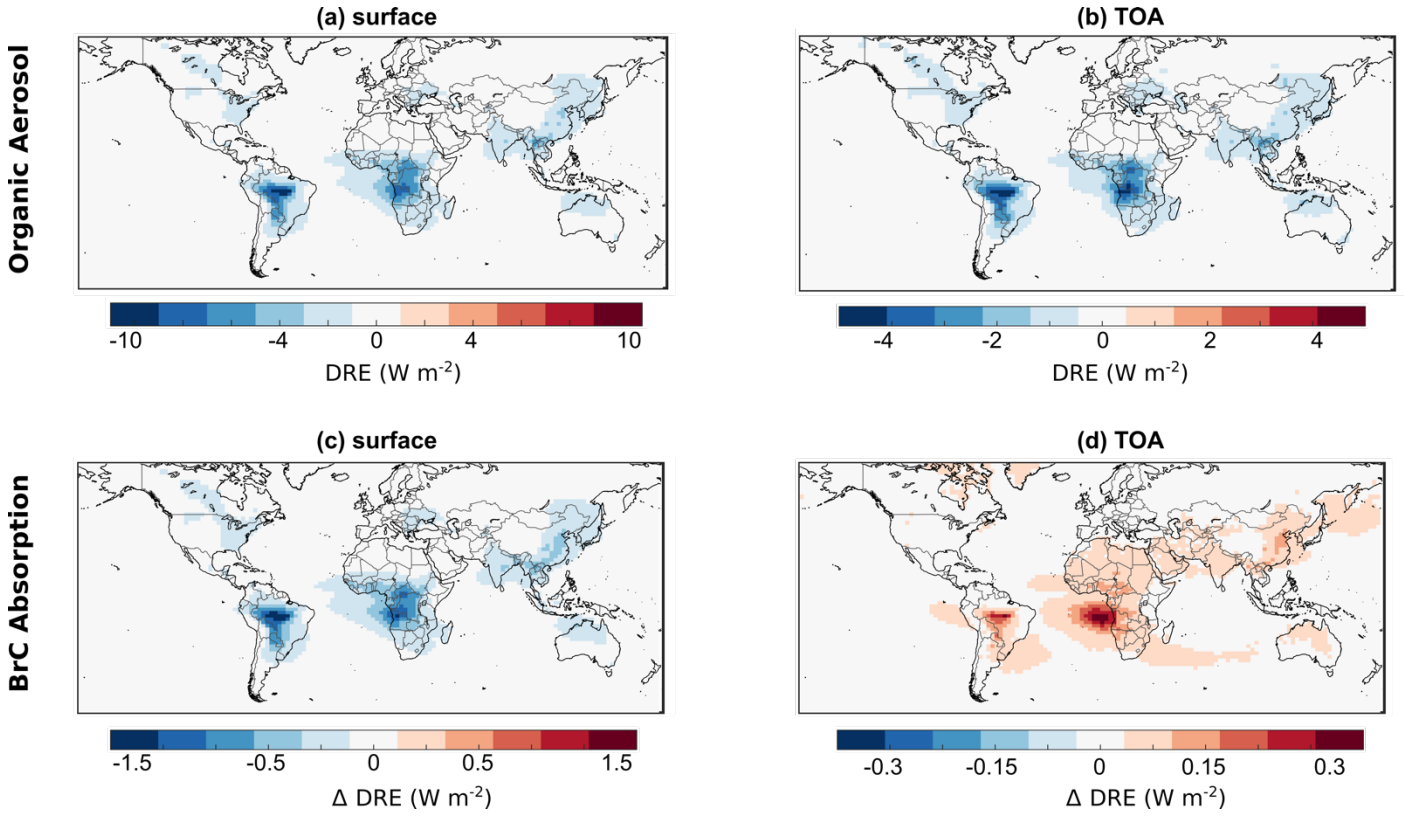

Figure 6: Annual mean all-sky DRE values for 2007 (Wm^{-2}). The top two panels are the DRE values for organic aerosol from the case 2 simulation including BrC at a) the surface and b) TOA. The bottom two panels are the change in DRE values for absorption by BrC calculated as the difference between the DRE values for organic aerosol from the case 2 simulation and the base case simulation (without BrC) at c) the surface and d) TOA.